# CRASHWORTHINESS ASSESSMENT IN AIRCRAFT DITCHING INCIDENTS

**C. Chandra*, T. Y. Wong* and J. Bayandor****

*** The Sir Lawrence Wackett Aerospace Centre**
**Royal Melbourne Institute of Technology, Melbourne, VIC, Australia**

****Center for Intelligent Material Systems and Structures**
**Virginia Tech, Blacksburg, VA, U.S.A.**
***E-mail: Bayandor@vt.edu***

**Keywords**: *Advanced Aerospace Design, Crashworthiness, Water Ditching, Smoothed Particle Hydrodynamics, Coupled Lagrangian-Eulerian*

## Abstract

*In this paper, a comparative study has been performed between the Meshless Lagrangian and Coupled Lagrangian-Eulerian schemes, to evaluate their overall efficiency and effectiveness for analyzing fluid-structure interactive systems. Soft body impact events onto composite laminates representing primary and secondary aircraft structures have been studied. Several cases with different bird velocities have been simulated to observe the non-linier behavior of soft body impact, along with the shortcomings of the modeling methodologies applied. The Meshless Lagrangian model produced a higher initial peak force, whereas the Coupled Lagrangian-Eulerian approach captured the impact window more smoothly with less obvious spikes. These schemes have also been compared with the conventional Lagrangian approach, which proved to be less accurate due to high mesh distortion and loss of mass from erosion. The study was further extended to analyze bird-strike on a composite wing leading-edge. With validation from experimental results, the developed modeling methodology was also used to analyze other fluid-structure interactive systems such as structural damage caused by aircraft ditching over water.*

## 1 Introduction

Composites are extensively used in modern aircraft structures due to their superior material properties, fatigue characteristics and design flexibility. However, with highly unidirectional properties, aerospace grade composites in particular are susceptible to impact damage and relatively brittle forms of failure. Damage due to soft body impact is of major concern because of the complexities it introduces in crashworthy analysis and design. Soft body impact is characterized by three stages which occur in quick succession. Initially, when the soft body comes in contact with the target structure, there is solid-structure interaction. At the instant of impact, a shock wave is generated, which propagates along the length of the soft body, crushing the internal structures of the bird. This causes a phase change within the soft body, resulting in its transformation from solid to fluid. Finally, the impact progresses as a fluid-structure interactive system, instigating further damage on the target structure. Current methods of studying fluid-structure interaction rely heavily on empirical data and experimentation. Such methods are usually too resource intensive and costly. Consequently, the use of explicit numerical modeling techniques can be considered as a practical alternative for analyzing soft body impacts. The three types of numerical modeling schemes that are commonly used to study such scenarios are the Lagrangian, Meshless Lagrangian and Coupled Lagrangian-Eulerian schemes. The Lagrangian scheme is a more conventional numerical approach, however in soft body scenarios can tend to produce less accurate results when mesh distortions become very large. The Meshless

Lagrangian and the Coupled Lagrangian-Eulerian schemes are able to overcome such inaccuracies, while imposing their own constraints. A comparison of Meshless Lagrangian and Coupled Lagrangian-Eulerian schemes is therefore necessary to better identify the specific applications of each analysis method. Peak forces experienced and impact damage sustained by structures constitute two of the major parameters in analysis of fluid-structure interactive systems. As part of this study, a flat panel and a leading edge, representing aircraft primary and secondary structures respectively, have been used to analyze different soft body impact scenarios. Peak forces as well as progressive impact damage traces have been compared between the two methods to provide a more detailed understanding of each scheme.

## 2 Nomenclature

$C$ = Constant of normalization for kernel function
$D$ = Bird diameter
$L$ = Bird overall length
$P$ = Pressure in shock region
$P_s$ = Stagnation pressure
$W$ = Smoothing kernel

$b$ = Specific body force vector
$c$ = Convective velocity
$h$ = Length of cylindrical portion of bird model
$\bar{h}$ = Smoothing length
$r$ = Bird radius
$u_o$ = Impact velocity
$u_p$ = Particles velocity in soft body
$u_s$ = Shock velocity
$v$ = Particle velocity
$v_m$ = Mesh velocity

$\rho$ = Bird density
$\sigma$ = Cauchy stress tensor
$\theta(y)$ = Auxiliary function for smoothing kernel
$\prod^h u$ = Particle approximation for Meshless Lagrangian particles.

## 3 Physics of Impact

As a soft body collides with a target, it experiences a phase change. Wilbeck [1] explained this phenomenon based on the hydrodynamics theory, which included impact initiation, shock wave and subsequent release wave formations, steady flow condition and impact termination. In his hypothesis, front interacting particles of the soft body may reduce to zero velocity immediately when come in contact with the target surface. Given a high enough relative impact velocity, a shock wave is then formed, propagating within the soft body. The formed shock wave brings succeeding particles of the soft body to rest and compresses the impactor's constituent material as it progresses through the soft body. As the pressure within the compressed region increases drastically, it exceeds the strength of material and triggers a solid to fluid phase transition. Subsequently, the material in the path behind the shock wave transforms to a fluidic bulk and can be treated as a non-Newtonian fluid (or Newtonian in an idealized modeling platform). Considering reasonable rigidity of the target, the particle velocity in the soft body, $u_p$, will be equivalent to the impact velocity, $u_o$. Applying conservation of mass and momentum theories, pressure in the shock region can be expressed as:

$$P = \rho_1 u_S u_o \qquad (1)$$

After the shock initiation, the higher energy portion of the shock propagates backwards along the soft medium of the projectile. Due to the circumferential pressure difference within the projectile, soft body particles, now in fluidic state, accelerate radially outward. This is instigated through the formation of a series of release waves. The lateral and then longitudinal propagations of the release waves reduce the pressure in the compressed region of the soft body and thus weaken the rebound shock velocity. This process continues until the shock dissipates and a steady flow condition is established. For an impact on a rigid plate, a stagnation point exists at the centre of the target. The stagnation point has a corresponding zero velocity and a

stagnation pressure, $P_s$. Assuming that the fluid is incompressible, stagnation pressure can be expressed as:

$$P_s = \rho_1 u_o^2 / 2 \quad (2)$$

Once the pressure release waves reach the end of the soft body, the remainder of the projectile continues to move toward the target in a steady fashion until the impact is terminated.

## 4 Numerical Modeling Schemes

To analyze soft impact, there are three established methods of numerical modeling adapted widely by researchers: Lagrangian, Meshless Lagrangian and Coupled Lagrangian-Eulerian schemes. Different schemes use different governing theories, which have their own advantages and disadvantages.

### 4.1 Lagrangian Scheme

The Lagrangian scheme is a mesh intensive numerical approach. In this scheme, individual nodes of the computational mesh follow their associated material movements within a Lagrangian framework [2]. The material domain ($R_X$) and spatial domain ($R_x$) are two key elements that define this framework.

The motion of the material in the material domain can be mapped into the spatial domain by a mapping function, $\varphi$ , and material velocity ($v$). Their mathematical representations are expressed through Eqs. (3) and (4), respectively.

$$\varphi(X,t) = (x,t) \quad (3)$$

$$v(X,t) = \left.\frac{\partial x}{\partial t}\right|_x \quad (4)$$

When the material coordinates are fixed, the material velocity can be determined using Eq.(4). This facilitates the tracking of the material motion. Since the material grid is the same as the spatial grid, the scheme supports time history dependent constitutive relations.

### 4.2 Meshless Lagrangian Scheme

In the Meshless Lagrangian scheme, the material is represented by a set of discrete particles, where the velocity vector for each particle is related to the rest of the particle field through a flexibility matrix, unlike the Lagrangian scheme that relates the displacement in each node to the traction in other nodes through the stiffness matrix. A significant advantage of this scheme is the *adaptive* nature (i.e., resolution of solution is automatically adapted to suite local environment) of particle approximations. Due to its specific formulation, the scheme is not affected by arbitrariness of particle distribution [3]. Since this method is mesh-free, it is favored over traditional FEM for problems involving large structural distortions.

Numerically, the soft body can be represented as a cluster of particles moving at the flow velocity. Each of the Meshless Lagrangian particles symbolizes an interpolation point on which all material properties are known. The solution in its entirety is then calculated on every particle with a regular interpolation function, called the smoothing length. The equations of conservation of momentum are then equated to fluxes or inter-particular forces to obtain the final solutions [4]. A summary of the theory behind particle methods and approximations to the smoothing function is given below [3,4].

Let $S$ be a set of particles, $x_i(t)$ be the location of particle $i$, and $w_i$ ($t$) be its weight. Particle methods for moving particles are based on quadrature formulae. The quadrature formula can be written for this case as,

$$\int_\Omega f(x)dx \approx \sum_{j \in P} w_i(t) f(x_j(t)) \quad (5)$$

Relating the idea of smoothing kernels, an approximation of the function can be made. An auxiliary function $\Theta$ can be introduced to define the smoothing kernel. The most suited function for Meshless Lagrangian analysis is the cubic B-spline function, which provides suitable regularity. This is given by Eq. (6), and is graphically represented in Fig. 1.

$$\theta(y) = C \times \begin{cases} 1 - \frac{3}{2}y^2 + \frac{3}{4}y^3 & for \quad y \le 1 \\ \frac{1}{4}(2-y)^3 & for \quad 1 < y \le 2 \\ 0 & for \quad y > 2 \end{cases} \qquad (6)$$

In Eq. (6), $C$ is the constant of normalization, which depends on the space dimensions.

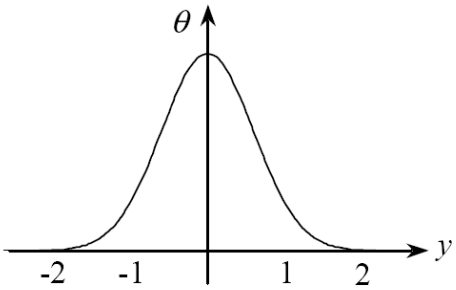


Fig. 1. Cubic B-spline type auxiliary function

The smoothing kernel $W$ is then defined as,

$$W(x_i - x_i, \bar{h}) = \frac{1}{\bar{h}}\theta\left(\frac{x_i - x_i}{\bar{h}}\right) \qquad (7)$$

In Eq. (7), $W(x_i - x_i, \bar{h}) \to \delta$ when $\bar{h} \to 0$, where $\delta$ is the Dirac function, $\bar{h}$ is the smoothing length of the kernel. The particle approximation $\prod^h u$ is then given by,

$$\prod^h u(x_i) = \sum_{j \in \Omega} w_j(t) u(x_j) W(x_i - x_j, \bar{h}) \qquad (8)$$

where $\prod^h$ is the virtual viscous pressure, allowing the singular peak forces, initiated by individual particles, to be smeared over the impact region.

The smoothing length represents a mean value of distance between elements $i$ and $j$. Over time, it has been shown that this approximation can lead to unstable results. A reasonable selection of smoothing length can be $\bar{h} = h(x_i)$, which is known as gather formulation. This means that the neighbors for any given particle are included in a sphere centered at $x_i$ with a radius of $h(x_i)$.

### 4.3 Coupled Lagrangian-Eulerian

Figure 2a shows a schematic of the Lagrangian scheme. The Lagrangian scheme is capable of tracking free surfaces and interfaces between different materials. The scheme also facilitates history dependent constitutive relations. However, Lagrangian scheme treats each particle in the mesh as an individual. Particles move independent of each other and can diverge in space. The divergence can lead to excessive distortion of the Lagrangian mesh. There is also a possibility of mesh overlap [5], affecting the accuracy of the result.

The Eulerian scheme is also a mesh dependent approach. Individual nodes in the computational mesh in Eulerian frame are fixed [1]. Particles in the frame move with respect to the grid as shown in Fig. 2b. Eulerian scheme is capable of analyzing structures with large distortion. Particles cannot experience any overlapping since particles move in and with respect to the grid specified. However, the scheme is not able to trace movement of each individual particle.

Coupled Lagrangian-Eulerian is an approach to solve soft body problems using both Lagrangian as well as Eulerian reference frames. This technique is developed to minimize the limitations associated with using either scheme independently.

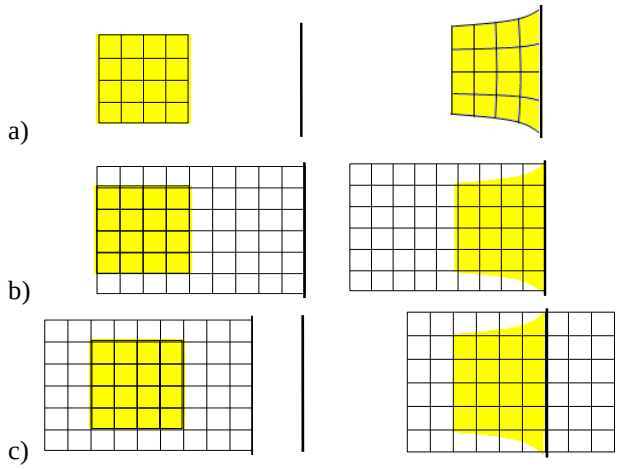


Fig. 2. Representation of a) Lagrangian, b) Eulerian, and c) Coupled Lagrangian-Eulerian schemes

Coupled Lagrangian-Eulerian is derived by using the combination of material time

derivative and grid time derivative into continuum mechanics governing equations. There are three domains in Coupled Lagrangian-Eulerian scheme: material domain, $R_X$, spatial domain, $R_x$, and reference domain, $R\chi$. The reference domain is introduced to identify grid points [1].

The reference domain is mapped into the material and spatial domains by $\psi$ and $\Phi$, respectively. Particle motion is defined by $\varphi$. Equation (9) expresses the relationship between the three mapping function. After mapping of all the domains, motion of the system can be determined. The relationship between material velocity, $v$, and mesh velocity, $v_m$, is defined by convective velocity, $c$. Convective velocity is the particle velocity as seen through the spatial domain.

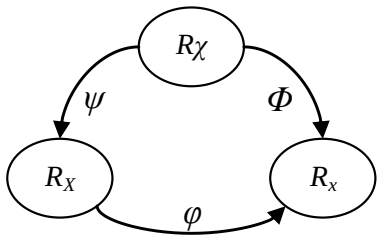


Fig. 3. Mapping of the three domains

$$\varphi = \phi \circ \psi^{-1} \tag{9}$$

$$c = v - v_m \tag{10}$$

If the material domain is equivalent to the grid reference domain, material and mesh velocity are equaled, and Lagrangian formulation is achieved. When the spatial domain is equivalent to the grid reference domain however, mesh velocity is zero and the convective velocity is equal to the material velocity as stated in Eq. (10), hence satisfying the Eulerian formulation. Therefore, in the Coupled Lagrangian-Eulerian scheme a proper relationship between the domains needs to be established so that a feasible solution can be obtained. Dealing with impact analysis, conservation of mass and momentum equations are applied. These equations can be expressed in the differential form as:

$$\begin{aligned} \left.\frac{\partial \rho}{\partial t}\right|_{\chi} + c \cdot \nabla \rho &= -\rho \nabla \cdot v \\ \rho\left(\left.\frac{\partial v}{\partial t}\right|_{\chi} + (c \cdot \nabla) v\right) &= \nabla \cdot \sigma + \rho b \end{aligned} \tag{11}$$

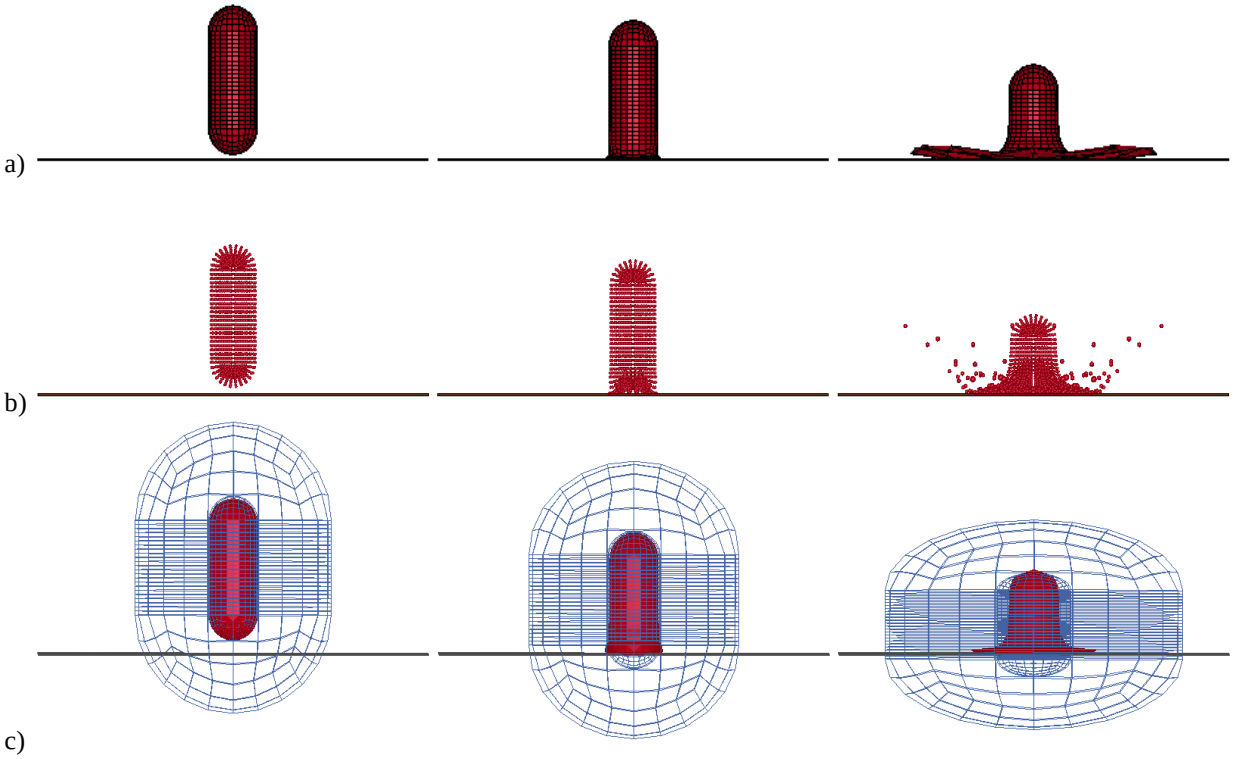


Fig. 4. Illustration of soft body impact on a rigid plate
a) Lagrangian b) Meshless Lagrangian c) Coupled Lagrangian-Eulerian

## 5 Bird and Target Modeling

Three types of artificial bird shapes are often used for bird strike analysis: straight ended cylinder, hemispherical ended cylinder, and ellipsoid [6]. Due to its advantages, in this paper hemispherical ended cylinder is adopted for calibration and analysis purposes [7]. Bird mass, density, $\rho$, and diameter, $D$ can be correlated using equations developed by Budgey [6]:

$$\rho = -0.063 \log_{10} mass + 1.148 \qquad (12)$$

$$\log_{10} D = 0.335 \times \log_{10} mass + 0.9 \qquad (13)$$

Setting the diameter of the bird model as 100 mm, the bird mass was determined as 1922 g for a density of 0.9411 g/cm$^3$. The dimensions of the bird were fixed by the set indicated in Eqs. (14). Once all the bird properties were determined, they were used Meshless Lagrangian and Coupled Lagrangian-Eulerian analytical schemes.

$$\begin{aligned} Volume &= mass/\rho \\ Volume_{cylinder} &= \pi r^2 h \\ Volume_{hemisphere} &= 4\pi r^3/6 \end{aligned} \qquad (14)$$

A flat primary aerospace panel and a leading edge were selected as targets representing an aircraft structure. They were constructed from composite laminates with a ply lay-up of $[0,45,90,-45]_2$. According to impact theory [1], target surface must be several times the diameter of the soft body. To ensure the target surface was sufficiently large, an 800 mm x 800 mm panel was used throughout the analysis. A representative leading edge model was also constructed using NACA 0012 aerofoil profile.

The both structures were clamped at four edges. The panel had a finer mesh density at the impact centre. The outer region of the panel had

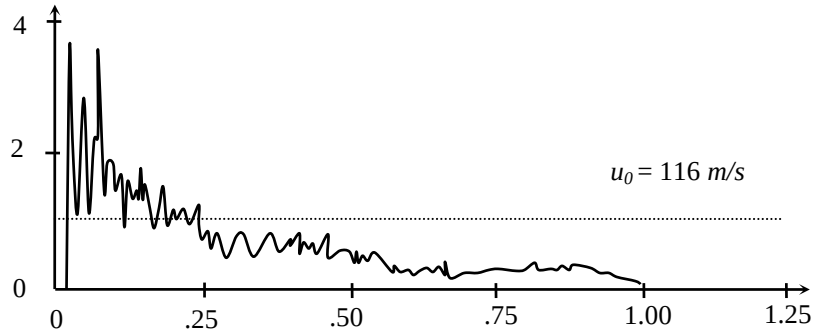


Fig. 5. Non- dimensionalized pressure with respect to time [1]

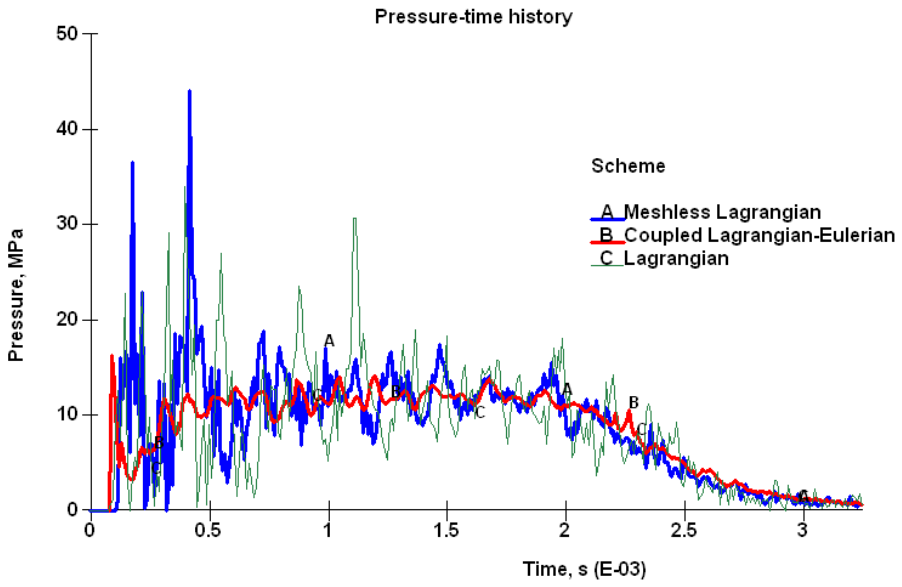


Fig. 6. Pressure with respect to time for Lagrangian, Meshless Lagrangian and Coupled Lagrangian-Eulerian scheme

a relatively coarser mesh. The fine and coarse mesh regions were bridged via a transition mesh zone [8]. The leading edge however modeled with a uniform mesh density.

## 6 Calibration of Numerical Bird Model

The numerical bird models in both analytical schemes were then calibrated against a rigid plate test data [1]. The numerical bird was set to impact onto the rigid plate at 116 m/s with the direction of impact set to normal. Figure 5 shows the experimental pressure-time history by Wilbeck [1], versus Fig. 6 that depicts the simulated pressure-time using both Meshless Lagrangian and Coupled Lagrangian-Eulerian schemes.

Comparison of the trends of both schemes with that of Wilbeck's underlies similar behavior. In agreement with the experimental results, the numerical birds in both approaches identified a peak pressure region at the moment of impact. Meshless Lagrangian scheme showed a higher peak pressure than the Coupled Lagrangian-Eulerian method. Past the peak pressure region, the impact pressure for both schemes dropped gradually until reaching zero at the end of the impact window. Both Meshless Lagrangian and Coupled Lagrangian-Eulerian schemes predicted the impact window within a reasonable margin of error. However, the Meshless Lagrangian scheme showed a more volatile variation in pressure after reaching the peak pressure than the competing scheme.

## 7 Results and Discussion

The impact scenario was analyzed for different bird velocities ranging from 75 to 100 m/s. Each scheme of modeling was then compared qualitatively for impact damage of target area, followed by a qualitative assessment of the impact force. The analysis was then extended to numerically model bird-strike on a wing leading edge.

### 7.1 Impact Damage Area

Significant damage to the target was observed at velocities closer to 100 m/s. The impact damage area is shown for each scheme in Fig. 7.

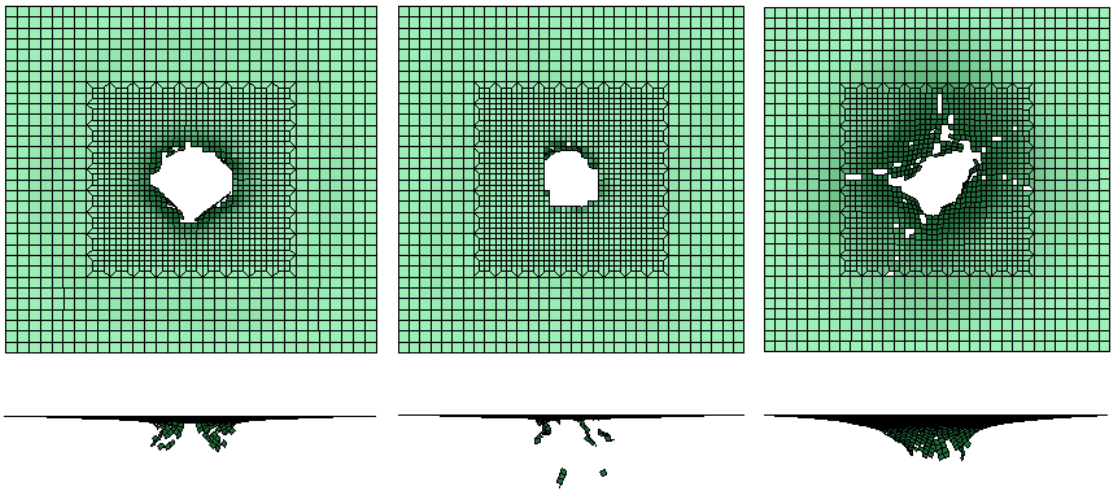

a) b) c)

Fig. 7. Impact damage at $u_0$ = 100 m/s and $t$ = 0.002 s
a) Lagrangian. b) Meshless Lagrangian. c) Coupled Lagrangian-Eulerian

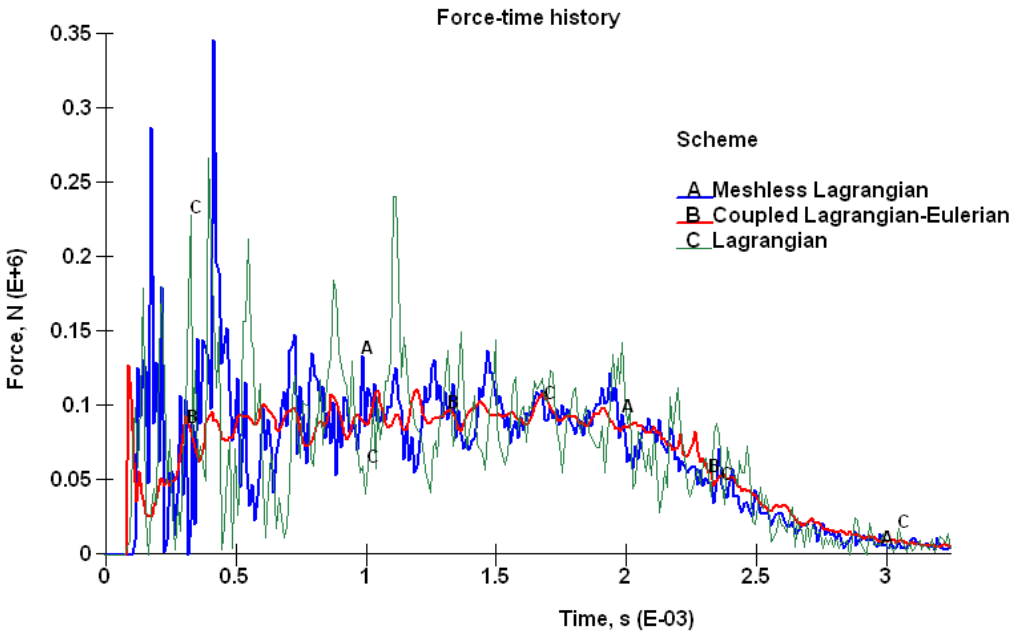


Fig. 8. Force-time history for all schemes at $u_0$ = 100 m/s

The impact damage trace detected on composite panels was rather different for each of the modeling schemes used. The damage areas identified by the Meshless Lagrangian method were the smallest for all cases considered, with the largest ones being those of the Coupled Lagrangian-Eulerian. Damage from the Lagrangian bird model was intermediate, despite the fact that the model suffered from unacceptable values of mass loss due to erosion and high mesh distortions after impact.

It was observed that the difference in damage areas in the three methods was mostly due to large variations in their predicted peak forces. The high peak forces for Meshless Lagrangian model caused immediate failure of the contact surface, leaving no leverage for the panel to yield.

## 7.2 Impact Force

Figure 8 shows the force-time history of each modeling scheme for impact on a flat plate at 100 m/s. The graph clearly identifies the peak forces at impact for each scheme. Forces at the moment of impact for the Lagrangian and Meshless Lagrangian bird models were respectively 48% and 110% larger than that of the Coupled Lagrangian-Eulerian model. This can well be a reflection of the nature by which each type of numerical bird model can interact with the target. For instance, the Meshless Lagrangian scheme is particle based, where as the Coupled Lagrangian-Eulerian approach treats the material as evenly distributed. This distinction in modeling approach can be a possible cause for large differences in peak

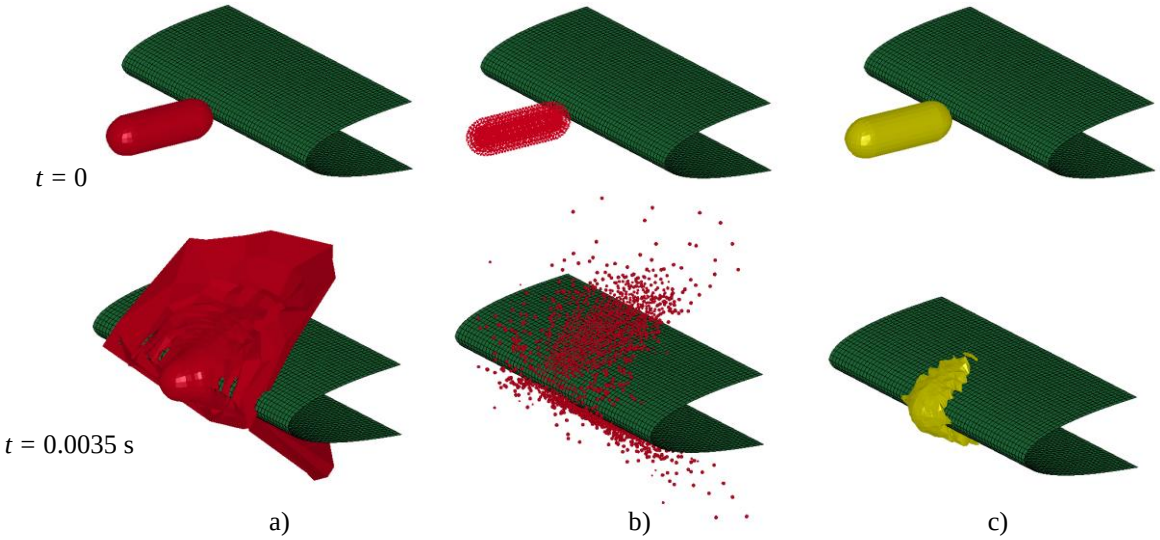


Fig. 9. Bird model impact on wing leading edge at $u_0$ = 75 m/s
a) Lagrangian b) Meshless Lagrangian. c) Coupled Lagrangian-Eulerian

forces, particularly if the smoothing length or the virtual viscous pressure (dealing with the inherent singularity problem of the method) have not been correctly identified.

Notwithstanding the fact that the Meshless Lagrangian scheme suffers from singularity induced errors and cannot identify contact areas, it is a robust scheme that can substitute and improve on the "fast aerospace design tools", which are mostly created based on the more conventional Lagrangian and Coupled Lagrangian-Eulerian approaches. The meshless method can further completely avoid discrepancies due to plasticity and material distortions.

The Lagrangian model showed irregularity throughout the impact regime. Erratic spikes of peak forces can be attributed to high mesh distortion after the initial impact phase. This sporadic behavior can further be exacerbated by material erosion and time-scaling, which was initially introduced to promote contact stability.

### 7.3 Wing Leading Edge

Figures 9 and 10 show the impact of bird model for all three modeling schemes. The previous arguments on using the three methods in modeling impact scenarios onto the primary aircraft panels remain valid. Further, when dealing with curved targets, it has to be noted that mesh distortion in pure Lagrangian models is overly large, rendering the results of soft impact analyses using this method unacceptable.

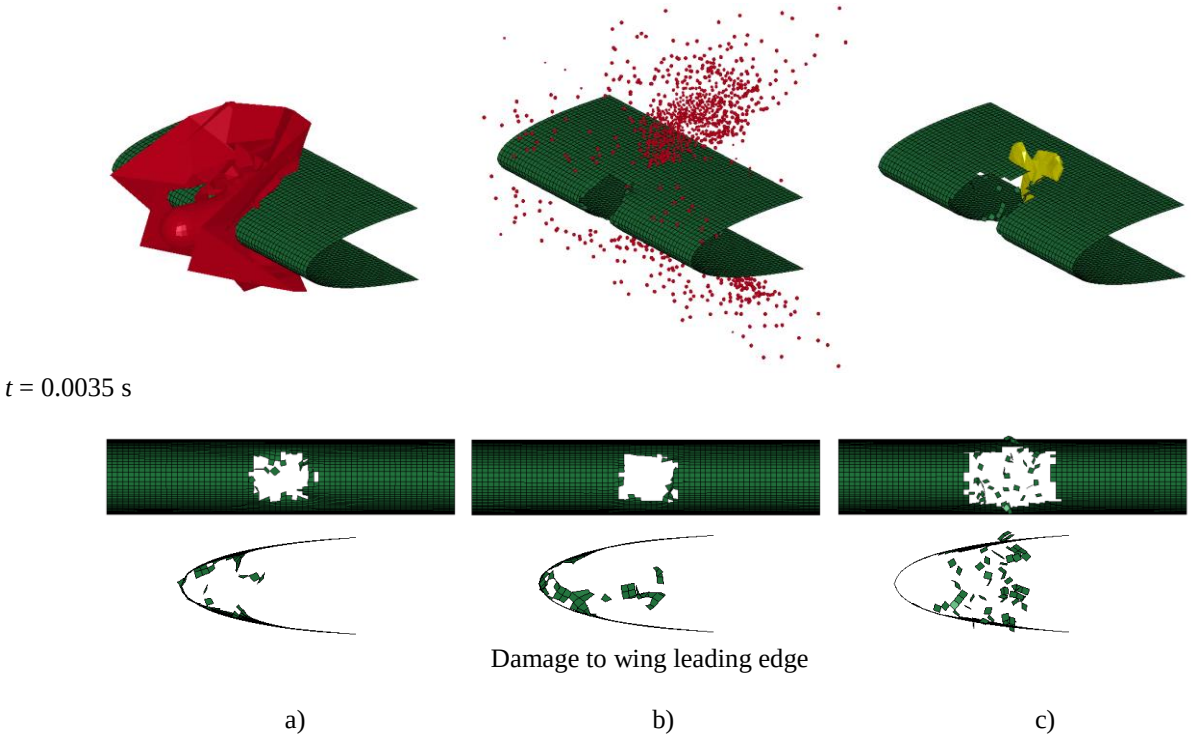


Fig. 10. Impact damage to wing leading edge at $u_0$ = 100 m/s
a) Lagrangian. b) Meshless Lagrangian. c) Coupled Lagrangian-Eulerian

## 8 Aircraft Ditching

In the aviation history, there has been a very few open reports on known cases of large commercial passenger jets surviving emergency water landing. This is except for the landing of the Airbus A-320 under the banner of US Airways Flight number 1549 and the command of Captain Chesley Sullenberger over Hudson River in January 15, 2009, success of which would have to be mostly attributed to the remarkable pilot's skills and his calm, yet calculated conduct. This incident and other reported or unreported accidents alike, call for further research in the area of soft collision during the Technology Readiness and Aircraft Design phases. This necessity is further justified as passenger safety, particularly for large airliners, is of paramount. Given the resource intensiveness and high costs associated with field trials, it is almost impractical to obtain pre-detailed design experimental data using full scale, fully functional prototypes or even scaled models to assess the crashworthiness of concept aircraft designs in possible soft crash scenarios. Developing an accurate modeling methodology that can numerically examine aircraft ditching incidents over water can assist manufacturers tremendously in designing improved and safer aerospace structures.

The ditching scenario can be categorized as soft crash, an event typical of fluid-structure interaction. As part of this study, a preliminary analysis was conducted on aircraft ditching using the Meshless Lagrangian scheme. Figure 11 shows the model of a generic large passenger jet constructed with shell elements, having an approximate weight of 52 tons. This model was assigned an initial pitch of -10$^{o}$ with a resultant velocity of 118 m/s. Figure 11 also depicts the body of water containing 360,000 equally distributed Meshless Lagrangian elements.

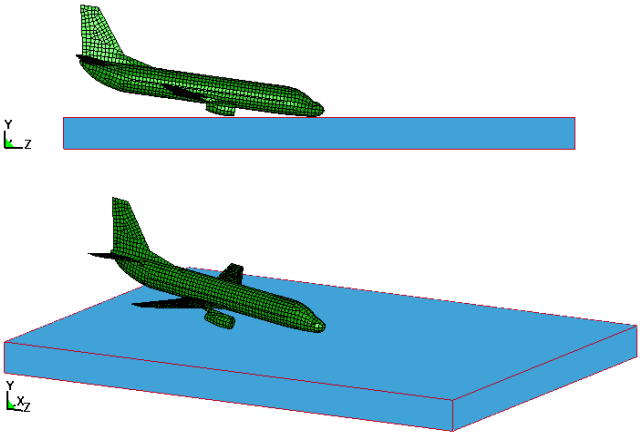

Fig. 11. Numerical model for aircraft ditching analysis

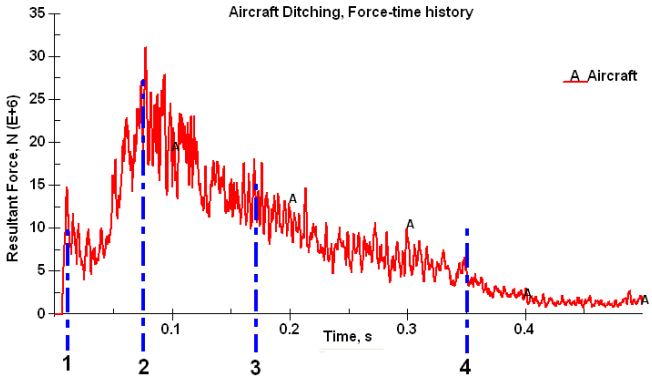


Fig. 12. Aircraft ditching force-time history

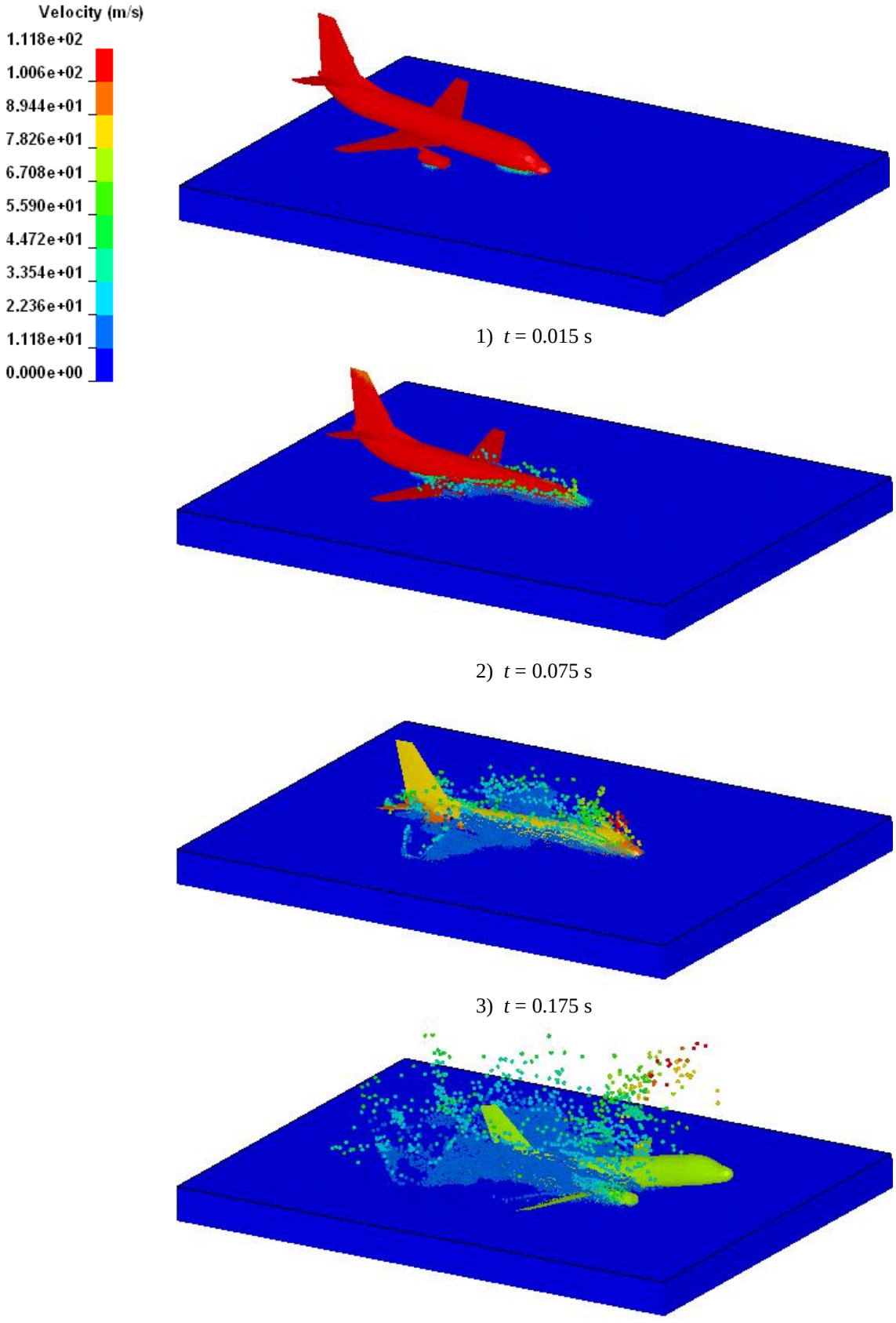


1) $t$ = 0.015 s

2) $t$ = 0.075 s

3) $t$ = 0.175 s

4) $t$ = 0.350 s

Fig. 13. Resultant velocity contours for an aircraft ditching scenario

Figure 12 shows the force-time history for a time period of 0.5 s. The aircraft experiences an initial impact force of nearly 15 MN, which peaks to a maximum of around 32 MN at 0.075s. The maximum force is observed when the center portion of the fuselage impacts the water. This is due to the obviously much larger impact area (now including the center of the fuselage and the area of the wings) and perhaps an added force from pitching rotation induced by the initial impact and the aircraft buoyancy. Figure 13 shows the resultant velocity contours pertaining to the four timelines marked in Fig. 12.

## 9 Conclusion

This paper presents a comparative study between the Meshless Lagrangian and Coupled Lagrangian-Eulerian schemes in an explicit finite element platform, to evaluate their overall efficiency in analyzing fluid–structure interactive systems. In particular, the focus was initially given to bird-strike events as an apparent candidate for less computationally intensive soft-body impact. The two methods were further compared with the typical Lagrangian approach to benchmark their advantages and shortcomings against a well established technique. Following a parametric study and calibration of the numerical bird model, a series of simulations was carried out for various impact velocities ranging from 75 to 100 m/s, using aerospace composite primary laminate panels as the target. At higher velocities, the impact damage traces detected by Lagrangian and Meshhless Lagrangian schemes were not as widespread as for the Coupled Lagrangian-Eulerian model. This was attributed to the higher peak forces predicted by both Lagrangian based models, due to which the target elements failed immediately leaving no time for the panel to yield.

The Lagrangian model suffered from high mesh distortion and erosive mass loss, rendering it an unfavorable candidate for soft impact modeling. In the Coupled Lagrangian-Eulerian scheme, the material was distributed evenly throughout the impactor, unlike the Meshless Lagrangian approach, where the model was discrete and particle based. This allowed the Coupled Lagrangian-Eulerian scheme to capture the impact window more smoothly. This was not the case for Meshless Lagrangian where instabilities were recorded all through the impact regime. These spikes can be reduced by introducing a stronger pressure distribution function that can smear the nodal pressures more efficiently throughout the model.

Continuing studies will aim to further experimentally validate the selected numerical scheme. The subsequently improved soft impact modeling methodology will then be used to extend the scope of the current work and investigate other fluid-structure interactive systems of interest. Soft crash scenarios, encompassing aircraft water ditching, are in this category, with an example of initial undertaking in this area presented in section 8.

## 10 Acknowledgments

The authors would like to thank and acknowledge the valuable input from Dr. Bayandor's Dynamic Damage Modeling research team. In particular, the authors wish to acknowledge the great assistance provided by A. Zammit, M. Kim, M. Chishti, and S. Shah throughout the life of this project.

## References

[1] Wilbeck JS. *Impact behavior of low strength projectiles*, AFML TR-77-134, 1978.

[2] Donea J, Huerta A, Ponthot JPh. and Fodríguez-Ferran A. *Chapter 14 Arbitrary lagrangian-eulerian methods*, Encyclopedia of Computational Mechanics, URL: http://www.wiley.co.uk/ecm/pdfs/Volume_1_Chapter_14.pdf , 2004.

[3] Lacome JL. *Smooth particle hydrodynamics (SPH): a new feature in ls-dyna*, Immeuble AEROPOLE - Bat 1, Blagnac, 2000.

[4] Liu GR and Liu MB. *Smoothed particle hydrodynamics a meshfree particle method*, World Scientific, 2003.

[5] Carlton A. *A summary study on arbitrary lagrangian-eulerian: methodology, implementation, and application, summer research experience for undergraduates*, Oregon State University, URL: http://wave.oregonstate.edu/Education/REU/2004_REU/Carlton.pdf , 2004.

[6] Budgey R. The development of a substitute artificial bird by the international birdstrike research group for use in aircraft component testing, *International Bird Strike Committee*, IBSC25/WP-IE3, Amsterdam, 2000.

[7] Bayandor J, Johnson A, Thomson RS, Joosten M. Impact damage modelling of composite aerospace structures subject to bird-strike, *The 25th Congress of the International Council of the Aeronautical Sciences*, ICAS 2006, Hamburg, Sept. 2006.

[8] Joosten M., Bayandor J. Coupled SPH composite cohesive damage modeling methodology for analysis of solid-fluid interaction, The 46th AIAA Aerospace Sciences Meeting and Exhibit, Reno, Jan. 2008.

## Copyright Statement